ORIGINAL ARTICLE

Thermal conversion behavior of paper mill sludge: characterization, kinetic, and thermodynamic analyses

Ali Yaras[1] · Bilal Demirel[2] · Fatih Akkurt[3] · Hasan Arslanoglu[4]

Abstract

The present paper reports the pyrolysis behavior, kinetic, and thermodynamic parameters of paper mill sludge (PMS), which is a paper manufacturing residue and cannot be re-evaluated, at three heating rates (5, 10, and 20 °C min^{-1}) under non-isothermal conditions. Ultimate and proximate analyses of the paper mill sludge were carried out. Kinetic and thermodynamic parameters were calculated using four model-free methods; Flynn-Wall Ozawa (FWO), Friedman, Kissinger-Akahira-Sunose (KAS), and distributed activation energy model (DAEM). High R^2 values revealed that all models are compatible with TGA data. The activation energy calculated (101.01 kJ mol^{-1}) from FWO was higher than the other three methods. Pre-exponential factor values ranged from 0.56×10^3 and 14.55×10^3 s^{-1} for all methods. Kinetic and thermodynamic findings will be beneficial in terms of the process design of PMS pyrolysis.

Keywords Paper mill sludge · Pyrolysis · Model-free kinetics · Thermogravimetric analysis · Thermodynamic parameters

1 Introduction

The demand for paper and paper products is increasing day by day in the world, especially in China and India [1]. For

Highlights
• A survey on thermal degradation, kinetic, and thermodynamic analysis of paper mill sludge.
• Activation energy was estimated for FWO, Friedman, KAS, and DAEM methods.
• Thermodynamic parameters for paper mill sludge pyrolysis were calculated.
• Findings will be beneficial in terms of the process design of PMS pyrolysis.

✉ Ali Yaras
aliyaras@bartin.edu.tr; ayaras01@gmail.com

1 Department of Metallurgy and Material Engineering, Faculty of Engineering, Architecture and Design, Bartın University, 74110 Bartin, Turkey

2 Department of Material Science and Engineering, Faculty of Engineering, Erciyes University, 38039 Kayseri, Turkey

3 Department of Chemical Engineering, Faculty of Engineering, Gazi University, 06680 Ankara, Turkey

4 Department of Chemical and Process Engineering, Faculty of Engineering and Architecture, Ahi Evran University, Kırsehir, Turkey

instance, about 3% of the world's paper production is carried out in India, with an annual production of one million tons of paper [2]. Paper products are manufactured following a series of mechanical and chemical processes, and massive amounts of wastewater, solid, and sludge are released [3]. Paper mill sludge (PMS), one of these wastes, is released during wastewater treatment and contains various organic and inorganic components, and the fact that it is not properly managed is a serious potential threat to the environment and ecology [3]. It is generally known that approximately 50 kg of PMS (dry based) is generated for one ton of paper manufacturing [4]. PMS has dispatched landfills for permanent disposal following the filtration process, but limited storage areas and stringent environmental regulations/laws complicate that. Another disposal option is incineration. However, it is not sustainable and feasible due to the high process cost, the complex content of PMS, and the formation of greenhouse gas emissions [5]. As that, the USA and European countries have serious limitations on disposal and waste management [3]. Therefore, the disposal/evaluation of PMS with safe and innovative technology has become an important issue in terms of sustainable environment and production [1, 6].

Previous researchers have reported the following alternative evaluation techniques for PMS; production of clay bricks [7] and ceramic tiles [8], clinker production [9], mortar preparation [10], activated carbon [11], and adsorbent [12].

However, energy production in the form of biogas and biofuel from paper mill sludge is an eco-friendly approach in terms of reducing the waste load and waste disposal cost of the paper manufacturing facility and meeting environmental regulations [13]. In this sense, seeking to find the best method for sustainable bioenergy production from this PMS is ongoing. Ahmed and Gupta [14] examined the methods of pyrolysis and gasification for energy production from PMS and found that gasification was more effective than pyrolysis. On the other hand, thanks to the biogas production from PMS, the energy costs of the heating units in the facilities are reduced and this energy can be utilized to dry the feedstock [15]. As is seen, thermochemical treatments are of great interest not only in processing this industrial waste but also in converting it into green energy. Pyrolysis, gasification, and combustion processes are classified according to the reactive atmosphere and operating temperature. In terms of combined heat and power generation, combustion is a more preferred method compared to pyrolysis and gasification [16]. In addition, by gasification of carbonaceous compounds in oxidative medium, combustible gases are released and ash is formed [17].

Organic materials can be converted into biochar (solid), pyrolytic oil (liquid) syngas products by pyrolysis [18, 19]. Also, the pyrolysis process requires low energy consumption than gasification [20]. Because of these, pyrolysis is more effective and eco-friendly compared to other thermochemical conversion methods [21, 22]. Conversion of lignocellulose based residues [23, 24], plastic wastes [25], and household bio-wastes [26] into energy and valuable chemical components using pyrolysis is one of the popular research topics of today. PMS contains various organic and inorganic components (Fe and Ca etc.) from the paper manufacturing process and wastewater treatment. With reference to the positive influence of Fe element on the syngas production [27], the presence of inorganic ions in PMS can also contribute to energy recovery during pyrolysis. The detailed information on the mechanism, kinetics, and thermodynamics of PMS pyrolysis is required for sustainable energy production with an eco-friendly approach in an industrial scale.

TGA analysis is an effective method to examine the thermal degradation behavior and thermal stability of various types of materials [28, 29]. Moreover, TGA data is used for mathematical modeling, which is critical for the design and optimization of thermochemical conversion reactors and processes [30, 31]. Two types of methods are commonly used to analyze TGA data; model-fitting method and model-free method. Of these, a model-free method is a simple approach by nature, and there is no risk of error in point of model selection and calculation of kinetic parameters [32]. The model-free method, which determines the kinetic parameters without any assumptions thanks to the different heating rate curves, also predicts the reaction mechanisms of complex materials [33]. These models (Kissinger-Akahira-Sunose (KAS), Flynn-Wall-Ozawa (FWO), Friedman and DAEM), known as iso-conversional, are applied at multiple-heating rates and produce lower margin of error (less than 1%). Also, these models only calculate the kinetic parameters of the process for particular conversion ranges (mostly 0.1–0.8) for an independent model.

Although there are considerable investigations on the thermal kinetics of various agricultural and industrial wastes (biomass), there is no detailed data on pyrolysis reaction kinetics of PMS. Therefore, the present paper focused to understand on the physicochemical properties, pyrolysis behavior, and kinetic analysis of PMS. Due to the possibility of peaks shifting at long interval in TG-DTG curves, the pyrolysis experiments were performed at short interval heating rates (5, 10, and 20 °C.min^{-1}) to clearly explain the thermal degradation phenomenon. Four model-free methods (Kissinger-Akahira-Sunose (KAS), Flynn-Wall-Ozawa (FWO), Friedman and DAEM) were studied for thermal analysis and following that the kinetic and thermodynamic parameters were calculated for each model. The physicochemical characteristics of PMS were determined by FTIR, ultimate/proximate analysis.

2 Material and method

2.1 Characterization of paper mill sludge

The paper mill sludge was supplied from a paper manufacturing plant in 2019. Before pyrolysis, PMS was dried at room temperature and then it was ground, sieved and the uniform particle sizes of less than 30 μm were obtained. The PMS powders were placed in a closed container for subsequent experiments.

The moisture, ash, and volatile matter contents (proximate analysis) of the PMS were determined according to E 1756 [34], E 1755 [35] and E 872 [36], respectively. The fixed carbon content was calculated by subtracting the sum of ash, moisture, and volatile matter from 100%. Ultimate analysis (carbon, hydrogen, nitrogen, sulfur, and oxygen content) of PMS was performed using the elemental analyzer (LECO CHNS 932). Functional groups in PMS structure were determined by FTIR analysis (Perkin Elmer Spectrum 100). FTIR analysis was performed with 4 cm^{-1} resolution in the 400–4000 cm^{-1} scanning range.

2.2 Thermogravimetric analysis

Thermal decomposition behavior of paper mill sludge pyrolysis was examined by thermal analyzer (FEI Quanta 250 FEG) under nitrogen gas atmosphere in the temperature range of 25–800 °C. The nitrogen flow rate was kept at 10 ml/min during the studied

temperature range. For each experiment, the initial amount of the paper mill sludge sample is 10 ± 0.2 mg. Pyrolysis was carried out at low heating rates (5, 10, and 20 °C.min^{-1}). For the accuracy of the results, the experiments were repeated at least three times. While TGA data contributed to the illumination of thermal degradation behavior of the materials, it also helped calculate the kinetic and thermodynamic parameters of the paper mill sludge pyrolysis process.

2.3 Kinetic analysis

Pyrolysis of lignocellulose-based wastes is a rather complicated phenomenon because of the wastes containing a wide variety of chemical components. A large number of reactions occur simultaneously during thermal decomposition, which is very difficult to predict reaction mechanisms. However, a reaction mechanism is suggested in the literature as follows [37];

Biomass (solid)$\xrightarrow{k(t)}$Volatile (gases + tar)

+ char (solid residue)
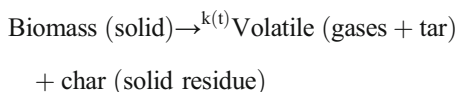
Assuming that the conversion of the raw material to the product is a single step process [38], the reaction rate constant (k) can be written according to the Arrhenius equation as follows;

$$k = Ae^{-\left(\frac{E}{RT}\right)} \tag{1}$$

where k, A (min^{-1}), E (kJ mol^{-1}), R (kJ mol^{-1} K^{-1}) and T (K) represent reaction rate constant, pre-exponential factor, activation energy, the universal gas constant, and absolute temperature, respectively. The conversion of raw material from the solid phase to the gas phase can be expressed by the following equation;

$$\frac{d\alpha}{dt} = k \, f(\alpha) \tag{2}$$

where α is the conversion rate, t is the time. The conversion expression is a function of temperature. Therefore, the conversion factor can be written as follows;

$$\alpha = \frac{W_o - W_t}{W_o - W_f} \tag{3}$$

where W_o is the initial weight of the sample, W_t is the weight of the sample at any given time, and W_f is the weight of the sample at the end of the pyrolysis process. The above equations can be combined as the following;

$$\frac{d\alpha}{dt} = Ae^{-(E/RT)}f(\alpha) \tag{4}$$

In terms of the uniform kinetic reaction, $f(\alpha)$ function can be given as follow;

$$f(\alpha) = (1-\alpha)^n \tag{5}$$

and with the combination of the abovementioned equations can be written the following;

$$\frac{d\alpha}{dt} = Ae^{-(E/RT)}(1-\alpha)^n \tag{6}$$

Heating rate (δ) is an effective parameter in the pyrolysis process and can be defined as follows;

$$\delta = \frac{dT}{dt} = \frac{dT}{d\alpha} X \frac{d\alpha}{dt} \tag{7}$$

The heating rate statement is replaced in the previous equation and simplified;

$$\frac{d\alpha}{dT} = \frac{A}{\delta} e^{-\left(\frac{E}{RT}\right)}(1-\alpha)^n \tag{8}$$

$$\frac{d\alpha}{(1-\alpha)^n} = \frac{A}{\delta} e^{-\left(\frac{E}{RT}\right)} dT \tag{9}$$

When the change equation of the conversion rate with temperature is integrated,

$$g(\kappa) = \int_0^\alpha \frac{d\alpha}{f(\alpha)} = \int_0^T \frac{A}{\delta} e^{-(E/RT)} dT \tag{10}$$

$$g(\kappa) = \frac{AE}{\delta R} \int_0^\alpha u^{-2} e^{-u} du = \frac{AE}{\delta R} p(\alpha) \tag{11}$$

where $g(\kappa)$ is the integral conversion and α is $\frac{E}{RT}$. Since there is no definitive solution of $p(\alpha)$, it can only be solved by the numerical approach method. In this sense, $p(\alpha)$ can be simplified according to the chosen approach method [39].

2.3.1 Flynn-Wall-Ozawa method

The Ozawa-Flynn-Wall method calculates the activation energy of the material based on the Doyle approach [40] as;

$$p(\alpha) = -2.315 + 0.457\alpha \tag{12}$$

Doyle's approach is put in an equation and rearranged;

$$ln(\delta) = ln\left[\frac{AE}{Rg(\alpha)}\right] - 2.315 - 0.457\frac{E}{RT} \tag{13}$$

For different heating rates, $ln(\delta)$ is plotted versus $1/T$ and linear line is obtained in the 0–1 conversion range. Activation energy is found from the slope of the line.

2.3.2 Friedman method

The Friedman method is one of the general iso-conversional methods used for thermal kinetic analysis of the material. In this method, the conversion function is constant and assumes that material degradation occurs only due to mass loss, independent of temperature. When the logarithms of both sides of the equation are taken,

$$ln\left(\frac{d\alpha}{dt}\right) = -\frac{E}{RT} + ln(Af(\alpha)^n) \tag{14}$$

The slope and intercept of the kinetic graph between $ln\left(\frac{d\alpha}{dt}\right)$ and $1/T$ gives $-\frac{E}{RT}$ and $ln(Af(\alpha)^n)$, respectively [41].

2.3.3 Kissinger–Akahira–Sunose method

Thermal kinetic parameters of the material are calculated according to the Kissinger-Akahira-Sunose (KAS) model with the following equation.

$$ln\left(\frac{\delta}{T^2}\right) = ln\left[\frac{AE}{Rg(\alpha)}\right] - \frac{E}{RT} \tag{15}$$

The activation energy and frequency factor can be determined using the slope and intercepts of $ln\left(\frac{\delta}{T^2}\right)$ versus $\frac{1}{T}$ graph [42].

2.3.4 Distributed activation energy model

Distributed activation energy model (DAEM) was developed to identify complex reactions that occur during pyrolysis and combustion of fossil fuels [43]. Apart from illuminating the complex reaction mechanisms of various biomass fuels, it was also widely used to determine the thermal kinetic parameters [44–46]. According to DAEM model, the activation energies of the first-order reaction and numerous irreversible parallel reactions during pyrolysis are related to the bond structure and strength [47]. On the other hand, DAEM model, which is preferred to examine the pyrolysis kinetics of various materials, is in harmony with experimental data, especially at low heating rates [45]. Simplified DAEM equation with reference to the Arrhenius equation;

$$ln\left(\frac{\delta}{T^2}\right) = ln\left(\frac{AR}{E}\right) + 0.6075 - \frac{E}{RT} \tag{16}$$

The left side of the equation $ln\left(\frac{\delta}{T^2}\right)$ against $\frac{1}{T}$ is plotted and a linear line is obtained. The slope is $\frac{E}{R}$ and intercept value is calculated from $ln\left(\frac{AR}{E}\right)$.

The calculation of thermodynamic parameters that are critical to determine the realization potential of a process is based on the following equations;

$$A = \frac{\alpha.E.exp\left(\frac{E}{R.T_p}\right)}{R.T_p^2} \tag{17}$$

$$\Delta H = E - R.T \tag{18}$$

$$\Delta G = E + R.T_p.ln\left(\frac{K_B.T_p}{h.A}\right) \tag{19}$$

$$\Delta S = \frac{\Delta H - \Delta G}{T_p} \tag{20}$$

where K_B, h, and T_p represent Boltzmann constant (1.381×10^{-34} J.K^{-1}), Plank constant (6.626×10^{-34} J s), and peak temperature (K) in DTG curve, respectively.

3 Results and discussion

3.1 Physicochemical analysis

The physico-chemical characteristics of PMS are given in Table 1. According to the data in Table 1, PMS contains less than 5% moisture; it can be considered to be a perfect raw material for pyrolysis and combustion processes [48]. Higher moisture content of raw material causes heat loss [49]. On the other hand, it has an amount of volatile compounds (22.70%wt.) and less ash content. The high ash content of raw material is known to cause insufficient combustion, increasing of operating cost, waste disposal problem, and low energy conversion [46, 50]. Therefore, the PMS is highly ignition performance. The high presence of fixed carbon (60.86%) in the PMS means that the heat production and energy value during the combustion are high. The results of the ultimate analysis in Table 1 show that PMS can be used as a biofuel for energy production due to its high carbon content (38.32%). Compared to the carbon content, it is close to the banana peel [51], hazelnut husk [31], and banana leaves [52]. The heating value of the PMS was determined at 29.84 MJ kg^{-1}. Another advantage of the PMS is that it does not contain high amounts of nitrogen and sulfur, which can cause harmful emissions such as SO$_x$ and NO$_x$ during pyrolysis and combustion reactions. As seen from Table 1, the nitrogen (0.38%) and sulfur (0.74%) content of the PMS is negligible. The data of the chemical analysis indicate that the PMS contains cellulose (57.25%) of high amount and lower percentage of hemicellulose (32.67%). The total cellulose and hemicellulose content is 89.92% that is a sign that the

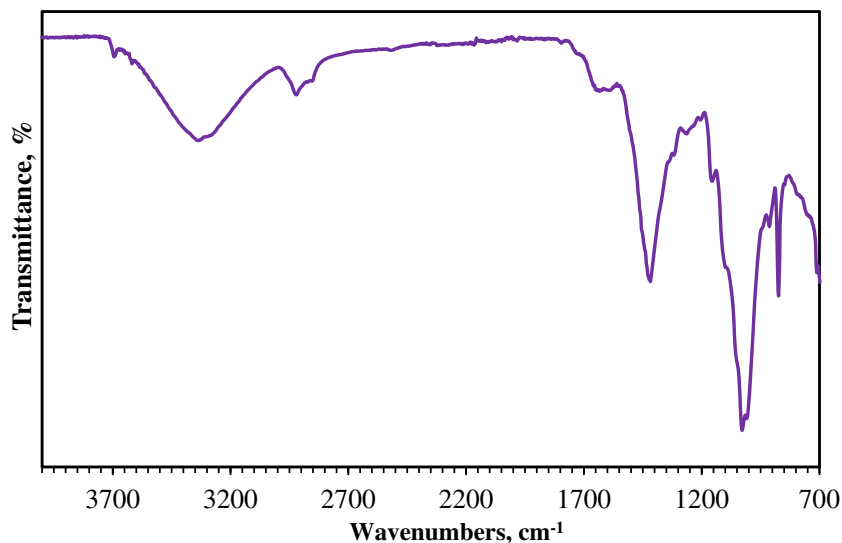**Table 1** Proximate, ultimate, and biochemical analysis of PMS

Ultimate analysis	(wt.%)	Proximate analysis	(wt.%)	Structure analysis	(wt.%)
C	38.32 ± 0.04	Moisture (at 105 °C)	1.79 ± 0.01	Cellulose	57.25
H	4.77 ± 0.04	Ash (at 950 °C)	14.65 ± 0.03	Hemi-cellulose	32.67
N	0.38 ± 0.02	Volatile matter (at 550 °C)	22.70 ± 0.14	Lignin	10.08
S	0.74 ± 0.05	Fixed carbon*	60.86 ± 0.06		
O*	39.35 ± 0.08				

*By difference

PMS is suitable for biofuel production. In addition, the presence of 10.08% lignin causes char formation following pyrolysis or combustion. The following order can be made for the thermal stability of the components in PMS; cellulose < hemicellulose < lignin [53].

3.2 FTIR analysis

The FTIR spectrum of the PMS in Fig. 1 presents very wide-ranging and extensive peaks. The peak at 3331 cm^{-1} is belong to the characteristic stretching –OH of cellulose [54]. The weak peaks in 2918 cm^{-1} and 2850 cm^{-1} which are between 2950 to 2800 cm^{-1} ranges are attributed to the C-H stretching of aromatic and aliphatic groups. Another signal at about 1640 cm^{-1} indicates the presence of C–O aldehyde group. The strong peak observed at 1417 cm^{-1} is caused by the presence of calcium carbonate. The strong peak observed at 1417 cm^{-1} indicates the presence of calcium carbonate, which is due to a large amount of calcite used during the paper manufacturing process. The vibrations of C–O–C bond and glucose stretching of C–O and OH could be seen at 1155 cm^{-1} and 1028 cm^{-1} signals, respectively. The other peak at 873 cm^{-1} represents the presence of the C–O–C bond [55].

3.3 Thermal degradation of PMS

With the pyrolysis process, the solid wastes can be converted into products in different physical forms. The type of raw material and reaction conditions is effective in the composition and amount of the products. Various and complex reactions occur during the pyrolysis of solid wastes. These reactions occur due to the breakdown of cellulose, hemicellulose, and lignin in the solid wastes to form different products.

The thermal degradation characteristics of the PMS under nitrogen atmosphere were determined by TGA analysis. TGA curve in Fig. 2 indicates that the PMS goes through three basic decomposition zones; dehydration (up to 150 °C), devolatilization (250–360 °C); and char formation (> 380 °C). In the first zone up to 160 °C temperature, low molecular weight compounds, and water molecules in PMS structure were removed. The highest weight loss occurred due to the thermal degradation of hemicellulose and cellulose in the range from 200 °C to 360 °C in the second region, also called the active pyrolytic region [56]. For the second zone, it is possible to say that hemicellulose and cellulose convert into lower molecular weight products with the increasing temperature. In this zone, volatile substance formation occurs as a result of two simultaneous exothermic processes of

Fig. 1 FTIR spectrum of paper mill sludge
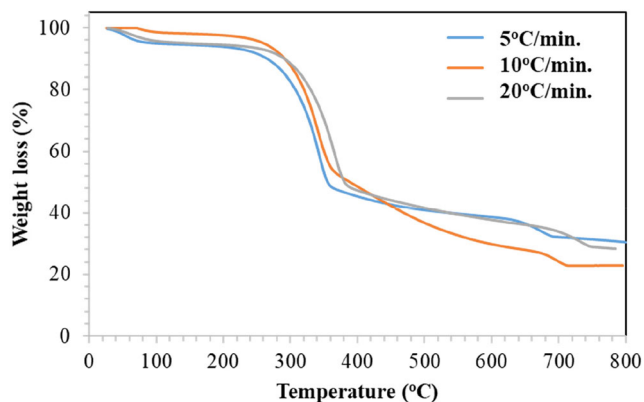
Fig. 2 TGA curves of paper mill sludge at different heating rates

hemicellulose, cellulose, and lignin degradation, respectively. Moreover, the maximum conversion (46.5%) was achieved in the temperature range from 260 °C to 360 °C in the second zone at 5 °C min⁻¹ heating rate. Hemicellulose decomposes at the lowest temperature (210–310 °C), followed by cellulose (310–390 °C) and lignin (from 160 to 800 °C). It is known that the thermal decomposition of cellulose occurs in two stages as follows; breaking chemical bonds into monomers and formation of carbon gases at low temperatures (up to 160 °C for the present study), and liquid formation due to bond integration at higher temperatures (350 °C for the present study) [57]. The third region in Fig. 2 is an endothermic phenomenon and belongs to lignin thermal decomposition at a higher temperature (> 360 °C) [58].

For DTG curves in Fig. 3, the first distinct peaks were observed at 240 °C, 250 °C, and 270 °C for 5, 10, and 20 °C.min⁻¹, respectively, quite likely due to the thermal degradation of hemicellulose. The straight and long-chain cellulose consisting of glucose monomers degraded in the temperature range 300 °C–390 °C and the maximum weight loss occurred at 390 °C [53]. The highest peak observed in the 300–400 °C range may be due to depolymerization and glycosidic linkage of lignocellulosic components [59]. As lignin degrades over a wide temperature range (160–800 °C), no clear boundaries for the decomposition of different
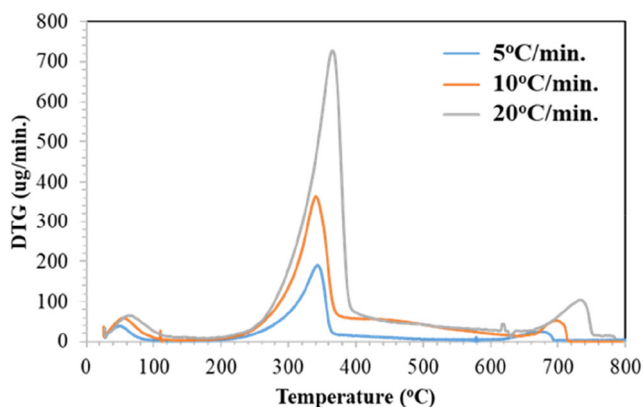
Fig. 3 DTG curves of paper mill sludge at different heating rates

components were observed [53]. When the PMS is evaluated in terms of content (Table 1), it can be indicated that the main decomposition peak is due to cellulose.

The characteristic parameters observed for different heating rates, especially the initial and peak temperatures, are given in Table 2. The zone where the main thermal degradation (260–620 °C) took place was divided into two sections. For heating rates of 5, 10, and 20 °C.min⁻¹ in the first section, T_i values are considered 270, 280, and 295 °C, while T_p and T_f temperatures are 310, 320, and 335 °C; 335, 340, and 350 °C, respectively. In the second zone, T_i, T_p, and T_f temperatures were seen as 365, 375, and 390 °C; 480, 500, and 515 °C; 585, 600, and 610 °C for heating rates of 5, 10, and 20 °C.min⁻¹, respectively. As a result, the increase of heating rate improved heat transfer limitations and TG-DTG curves shifted towards higher temperatures [60]. On the other hand, the increase of heating rate caused the peak temperature and degradation rate to raise even more; however, it did not affect the decomposition characteristic [61]. Finally, the release rates of volatile substances also increase to a certain extent with increasing heating rate.

3.4 Kinetic and thermodynamic analysis

Thermodynamic and kinetic parameters play a critical role in industrial scale in terms of reactor and process design [61]. Kinetic (pre-exponential factor and activation energy) and thermodynamic calculations (entalpy, entropy, free energy) were carried out for the 260–620 °C temperature range, where the main weight loss occurred. Model-free methods such as KAS, Flynn-Wall-Ozawa (FWO), and Friedman and DAEM were preferred for kinetic analysis. Activation energy, a measure of reaction reactivity, is defined as the minimum energy required to start a chemical reaction [62]. Except for 0.1 conversion rate, all conversion rates were compatible with the models due to the high correlation coefficient. According to the KAS, FWO, and Friedman and DAEM model, the average activation energy values were calculated as 37.73 kJ mol⁻¹, 101.01 kJ mol⁻¹, 46.16 kJ mol⁻¹, and 35.84 kJ mol⁻¹, respectively.

In addition, the activation energy calculated from the FWO method is higher than the other methods. The change of E values calculated for the FWO method reveals that it is not appropriate to explain the thermal degradation phenomenon by a single reaction mechanism. Significant variation of E values depending on the conversion rate in FWO method indicates that a multi-stage kinetics is effective for the PMS pyrolysis [59]. It is seen that the drastic changes of the activation energy are due to the components that prevent the decomposition of the volatile components as a result of thermal decomposition, and this phenomenon corresponds to the char formation zone in TGA curve. Also, the correlation coefficient, which is an indicator of model compatibility with

Table 2 TG-DTG characteristics parameters of PMS at heating rates of 5, 10, and 20 °C/min

Heating rates (°C/min)	Zone I (90–260 °C)				Zone II (260–360 °C)				Zone III (360–620 °C)			
	T_i (°C)	T_f (°C)	T_p (°C)	DTG (s^{-1})	T_i (°C)	T_f (°C)	T_p (°C)	DTG (s^{-1})	T_i (°C)	T_f (°C)	T_p (°C)	DTG (s^{-1})
5	95	220	160	0.00022	270	335	310	0.00035	365	585	480	0.00044
10	105	230	170	0.00027	280	340	320	0.00048	375	600	500	0.00058
20	110	240	185	0.00031	295	350	335	0.00059	390	610	515	0.00065

experimental data, is higher than 0.9 for each model as shown in Table 3. When the pre-exponential factories of all model-free methods are analyzed, they vary between 0.56×10^3 s^{-1} and 14.55×10^3 s^{-1}. The literature reports that the magnitude of A varies according to the reaction types in the pyrolysis process. When the A value is $< 10^9$ s^{-1} or in between 10^{10} and 10^{12} s^{-1}, the pyrolysis takes place as only the surface reaction or decomposition of cellulose, respectively. Also, a value higher than 10^{14} s^{-1} infers a high number of molecule collisions, which means that the pyrolysis process needs high

activation energy [58, 60, 63]. The pre-exponential factor calculated from FWO, Friedman, KAS, and DAEM models varies between 0.56×10^3 s^{-1} and 14.55×10^3 s^{-1}. Therefore, the pyrolysis of PMS takes place only as a surface reaction.

Thermodynamic parameters for conversion ratios between 0.2 and 0.8 are presented in Table 4. Enthalpy (ΔH) is a state function that shows that the reaction is endothermic or exothermic and reflects the decomposition of chemical bonds under constant pressure [64, 65]. The change of ΔH

Table 3 Activation energy and correlation coefficient estimates according to KAS, FWO, and Friedman and DAEM methods

Heating rates (°C/min)	α	KAS			FWO			Friedman			DAEM		
		Ea kJ/mol	A s^{-1} (*10³)	R^2	Ea kJ/mol	A s^{-1} (*10³)	R^2	Ea kJ/mol	A s^{-1} (*10³)	R^2	Ea kJ/mol	A s^{-1}	R^2
5	0.2	18.37	10.30	0.954	59.46	4.16	0.977	27.17	4.16	0.977	17.45	10.30	0.954
	0.3	39.05	5.89	0.999	106.24	8.80	0.999	48.55	8.80	0.999	37.09	5.89	0.999
	0.4	47.32	4.18	1.000	125.03	10.58	1.000	57.14	10.58	1.000	44.96	4.18	1.000
	0.5	54.16	2.81	1.000	140.45	12.00	1.000	64.19	12.00	1.000	51.45	2.81	1.000
	0.6	56.61	2.32	1.000	146.15	12.51	1.000	66.79	12.51	1.000	53.78	2.32	1.000
	0.7	43.31	4.91	0.994	117.38	9.95	0.996	53.64	9.95	0.996	41.14	4.91	0.994
	0.8	5.29	14.21	0.921	12.34	0.77	0.938	5.64	0.77	0.938	5.03	14.21	0.921
	Average	37.73			101.01			46.16			35.84		
10	0.2	54.05	3.20	1.000	138.96	11.48	1.000	63.50	11.48	1.000	51.35	14.15	1.000
	0.3	61.65	1.63	1.000	156.41	13.14	1.000	71.48	13.14	1.000	58.57	3.20	1.000
	0.4	66.83	0.59	1.000	168.26	14.22	1.000	76.90	14.22	1.000	63.49	1.63	1.000
	0.5	58.26	2.27	0.998	149.91	12.58	0.999	68.51	12.58	0.999	55.35	0.59	0.998
	0.6	26.71	8.37	0.960	81.34	6.52	0.979	37.17	6.52	0.979	25.37	2.27	0.960
	0.7	1.35	13.67	0.901	21.23	1.33	0.999	9.70	1.33	0.999	1.28	8.37	0.901
	0.8	2.97	13.95	0.991	19.88	1.22	1.000	9.09	1.22	1.000	2.82	13.67	0.991
	Average	31.63			86.52			39.54			36.89		
20	0.2	27.34	8.79	0.976	80.22	5.87	0.986	36.66	5.87	0.986	25.97	8.79	0.976
	0.3	46.27	4.86	1.000	122.96	9.92	1.000	56.19	9.92	1.000	43.95	4.86	1.000
	0.4	52.69	3.59	1.000	137.66	11.26	1.000	62.91	11.26	1.000	50.05	3.59	1.000
	0.5	56.80	2.79	1.000	147.12	12.09	1.000	67.23	12.09	1.000	53.96	2.79	1.000
	0.6	54.76	3.18	0.999	143.02	11.74	1.000	65.36	11.74	1.000	52.02	3.18	0.999
	0.7	31.64	7.50	0.976	92.82	7.45	0.986	42.42	7.45	0.986	30.06	7.50	0.976
	0.8	6.78	14.55	0.989	10.70	0.56	0.989	4.89	0.56	0.989	6.44	14.55	0.989
	Average	32.94			86.45			39.51			31.29		

Table 4 Thermodynamic parameter estimation of PMS at heating rates of 5, 10 and 20 °C/min

Heating rates (°C/min)	α	KAS			FWO			Friedman			DAEM		
		ΔH kJ/ mol	ΔG kJ/ mol	ΔS kJ/ mol K	ΔH kJ/ mol	ΔG kJ/ mol	ΔS kJ/ mol K	ΔH kJ/ mol	ΔG kJ/ mol	ΔS kJ/ mol K	ΔH kJ/ mol	ΔG kJ/ mol	ΔS kJ/ mol K
5	0.2	13.10	196.80	−0.290	54.20	242.67	−0.298	21.91	210.39	−0.298	12.45	186.96	−0.276
	0.3	33.78	220.42	−0.295	100.98	285.50	−0.291	43.29	227.81	−0.291	32.09	209.40	−0.280
	0.4	42.06	230.50	−0.298	119.77	303.33	−0.290	51.88	235.43	−0.290	39.96	218.98	−0.283
	0.5	48.90	239.44	−0.301	135.19	318.08	−0.289	58.92	241.82	−0.289	46.45	227.47	−0.286
	0.6	51.34	242.88	−0.303	140.89	323.56	−0.289	61.53	244.20	−0.289	48.77	230.74	−0.288
	0.7	38.04	225.64	−0.296	112.11	295.99	−0.290	48.38	232.25	−0.290	36.14	214.36	−0.281
	0.8	0.03	182.03	−0.287	7.08	204.45	−0.312	0.38	197.75	−0.312	0.02	172.93	−0.273
10	0.2	48.79	238.64	−0.300	133.69	316.82	−0.289	58.24	241.36	−0.289	46.35	226.71	−0.285
	0.3	56.39	249.79	−0.305	151.15	333.57	−0.288	66.22	248.63	−0.288	53.57	237.30	−0.290
	0.4	61.57	260.35	−0.314	163.00	345.00	−0.287	71.63	253.63	−0.287	58.49	247.33	−0.298
	0.5	53.00	244.66	−0.303	144.64	327.29	−0.288	63.24	245.89	−0.288	50.35	232.43	−0.288
	0.6	21.45	206.24	−0.292	76.08	262.18	−0.294	31.91	218.01	−0.294	20.37	195.93	−0.277
	0.7	−3.91	178.29	−0.288	15.97	210.45	−0.307	4.44	198.92	−0.307	−3.72	169.38	−0.274
	0.8	−2.30	179.80	−0.288	14.62	209.55	−0.308	3.82	198.75	−0.308	−2.18	170.81	−0.274
20	0.2	22.08	206.61	−0.291	74.95	261.61	−0.295	31.40	218.05	−0.295	20.97	196.28	−0.276
	0.3	41.00	228.66	−0.296	117.70	301.59	−0.290	50.93	234.82	−0.290	38.95	217.22	−0.281
	0.4	47.42	236.67	−0.299	132.40	315.63	−0.289	57.65	240.88	−0.289	45.05	224.84	−0.284
	0.5	51.54	242.11	−0.301	141.86	324.71	−0.289	61.97	244.82	−0.289	48.96	230.00	−0.286
	0.6	49.50	239.38	−0.300	137.76	320.77	−0.289	60.10	243.11	−0.289	47.02	227.41	−0.285
	0.7	26.37	211.74	−0.293	87.56	272.96	−0.293	37.16	222.56	−0.293	25.05	201.15	−0.278
	0.8	1.51	183.39	−0.287	5.43	204.42	−0.314	−0.38	198.61	−0.314	1.44	174.22	−0.273

calculated from KAS, FWO, and Friedman and DAEM models are as follows; 13.10–0.03 kJ mol⁻¹, 54.20–7.08 kJ mol⁻¹, 21.91–0.38 kJ mol⁻¹, 12.45–0.02 kJ mol⁻¹; 48.79–2.30 kJ mol⁻¹, 133.69–14.62 kJ mol⁻¹, 58.24–3.82 kJ mol⁻¹, 46.35–2.18 kJ mol⁻¹; 22.08–1.51 kJ mol⁻¹, 74.95–5.43 kJ mol⁻¹, 31.40–0.38 kJ mol⁻¹, 20.97–1.44 kJ mol⁻¹ for 5, 10, and 20 °C min⁻¹, respectively. As seen in Table 4, the change observed in ΔH due to the increase in conversion rate displays a trend similar to the change in activation energies. The increase of ΔH values means that the temperature rises, which means the breaking of strong chemical bonds in the PMS [65]. Consequently, according to all models, the positive ΔH values calculated for all heating rates and conversion rates reveal that the pyrolysis of PMS under the nitrogen atmosphere is endothermic and needs external energy [64].

Whether a chemical reaction occurs spontaneously and the direction of that reaction is defined by Gibbs free energy (ΔG) [64]. As shown in Table 4, ΔG values of KAS, FWO, and Friedman and DAEM models are 196.8 kJ mol⁻¹, 242.67 kJ mol⁻¹, 210.39 kJ mol⁻¹, 186.96 kJ mol⁻¹; 238.64 kJ mol⁻¹, 316.82 kJ mol⁻¹, 241.36 kJ mol⁻¹, 226.71 kJ mol⁻¹; 206.61 kJ mol⁻¹, 261.61 kJ mol⁻¹,

218.05 kJ mol⁻¹, 196.28 kJ mol⁻¹ for 5, 10, and 20 °C.min⁻¹, respectively.

The entropy (ΔS) refers to disorders. As presented in Table 4, entropy is negative for all conversion rates. It can be attributed that the irregularity degree of the products released after the pyrolysis process is higher than that of reactants. In addition, considering all heating rates and models, there was no remarkable differ in entropy changes.

4 Conclusions

Thermal degradation behaviors and pyrolysis kinetics of the PMS were quantified by thermogravimetric analysis. TG-DTG curves confirmed that the degradation peak with an increase of heating rate shifted towards the higher zone without changing the thermal decomposition characteristic of the PMS. While physicochemical testing indicated that the PMS has bioenergy potential, FTIR analysis confirmed the presence of beneficial functional groups in the raw material. According to the kinetic analysis, pyrolysis results are compatible with all models and these data provide great benefits in terms of optimization of pyrolysis conditions, design of process, and

reactor on an industrial scale. Consequently, industrial biomass with energy potential like the PMS can be utilized in sustainable and clean energy production.

Data availability The authors declare that all data and materials are available.

Compliance with ethical standards

Competing interests The authors declare that they have no competing interests.

Ethics approval and consent to participate Not applicable.

Consent for publication All authors declare that this manuscript is consent for publication.

References

1. Hu J, Zhang Q, Lee D-J (2018) Kraft lignin biorefinery: a perspective. Bioresour Technol 247:1181–1183

2. Bajpai P (2012) Environmentally benign approaches for pulp bleaching. Elsevier, Amsterdam

3. Cho D-W, Kwon G, Yoon K, Tsang YF, Ok YS, Kwon EE, Song H (2017) Simultaneous production of syngas and magnetic biochar via pyrolysis of paper mill sludge using CO2 as reaction medium. Energy Convers Manag 145:1–9

4. Bajpai P (2015) Generation of waste in pulp and paper mills. In: Management of Pulp and Paper Mill Waste. Springer, Amsterdam, pp 9–17

5. Zhao P, Ge S, Ma D, Areeprasert C, Yoshikawa K (2014) Effect of hydrothermal pretreatment on convective drying characteristics of paper sludge. ACS Sustain Chem Eng 2:665–671

6. Hu S, Ma X, Lin Y, Yu Z, Fang S (2015) Thermogravimetric analysis of the co-combustion of paper mill sludge and municipal solid waste. Energy Convers Manag 99:112–118

7. Vieira CMF, Pinheiro RM, Rodriguez RJS et al (2016) Clay bricks added with effluent sludge from paper industry: technical, economical and environmental benefits. Appl Clay Sci 132:753–759

8. dos Santos VR, Cabrelon MD, de Sousa TE, Quinteiro E (2019) Green liquor dregs and slaker grits residues characterization of a pulp and paper mill for future application on ceramic products. J Clean Prod 240:118220

9. Simão L, Jiusti J, Lóh NJ, Hotza D, Raupp-Pereira F, Labrincha JA, Montedo ORK (2017) Waste-containing clinkers: valorization of alternative mineral sources from pulp and paper mills. Process Saf Environ Prot 109:106–116

10. de Azevedo ARG, Alexandre J, de Xavier GC, Pedroti LG (2018) Recycling paper industry effluent sludge for use in mortars: a sustainability perspective. J Clean Prod 192:335–346

11. Gustafsson Å, Hale S, Cornelissen G, Sjöholm E, Gunnarsson JS (2017) Activated carbon from kraft lignin: a sorbent for in situ remediation of contaminated sediments. Environ Technol Innov 7:160–168

12. Oliveira G, Calisto V, Santos SM et al (2018) Paper pulp-based adsorbents for the removal of pharmaceuticals from wastewater: a novel approach towards diversification. Sci Total Environ 631: 1018–1028

13. Banerjee C, Dubey KK, Shukla P (2016) Metabolic engineering of microalgal based biofuel production: prospects and challenges. Front Microbiol 7:432

14. Ahmed I, Gupta AK (2009) Syngas yield during pyrolysis and steam gasification of paper. Appl Energy 86:1813–1821

15. Mohammadi A, Sandberg M, Venkatesh G, Eskandari S, Dalgaard T, Joseph S, Granström K (2019) Environmental performance of end-of-life handling alternatives for paper-and-pulp-mill sludge: using digestate as a source of energy or for biochar production. Energy 182:594–605

16. Manara P, Zabaniotou A (2012) Towards sewage sludge based biofuels via thermochemical conversion–a review. Renew Sust Energ Rev 16:2566–2582

17. Marrero TW, McAuley BP, Sutterlin WR et al (2004) Fate of heavy metals and radioactive metals in gasification of sewage sludge. Waste Manag 24:193–198

18. Black BA, Michener WE, Ramirez KJ, Biddy MJ, Knott BC, Jarvis MW, Olstad J, Mante OD, Dayton DC, Beckham GT (2016) Aqueous stream characterization from biomass fast pyrolysis and catalytic fast pyrolysis. ACS Sustain Chem Eng 4:6815–6827

19. Klemetsrud B, Ukaew S, Thompson VS, Thompson DN, Klinger J, Li L, Eatherton D, Puengprasert P, Shonnard D (2016) Characterization of products from fast micropyrolysis of municipal solid waste biomass. ACS Sustain Chem Eng 4:5415–5423

20. Neves D, Thunman H, Matos A, Tarelho L, Gómez-Barea A (2011) Characterization and prediction of biomass pyrolysis products. Prog Energy Combust Sci 37:611–630

21. Wang X, Deng S, Tan H, Adeosun A, Vujanović M, Yang F, Duić N (2016) Synergetic effect of sewage sludge and biomass co-pyrolysis: a combined study in thermogravimetric analyzer and a fixed bed reactor. Energy Convers Manag 118:399–405

22. Jin J, Li Y, Zhang J, Wu S, Cao Y, Liang P, Zhang J, Wong MH, Wang M, Shan S, Christie P (2016) Influence of pyrolysis temperature on properties and environmental safety of heavy metals in biochars derived from municipal sewage sludge. J Hazard Mater 320:417–426

23. Wang S, Dai G, Yang H, Luo Z (2017) Lignocellulosic biomass pyrolysis mechanism: a state-of-the-art review. Prog Energy Combust Sci 62:33–86

24. Chen W, Chen Y, Yang H, Li K, Chen X, Chen H (2018) Investigation on biomass nitrogen-enriched pyrolysis: influence of temperature. Bioresour Technol 249:247–253

25. Sharuddin SDA, Abnisa F, Daud WMAW, Aroua MK (2016) A review on pyrolysis of plastic wastes. Energy Convers Manag 115: 308–326

26. Vakalis S, Sotiropoulos A, Moustakas K, Malamis D, Vekkos K, Baratieri M (2017) Thermochemical valorization and characterization of household biowaste. J Environ Manag 203:648–654

27. Cho D-W, Lee J, Yoon K, Ok YS, Kwon EE, Song H (2016) Pyrolysis of FeCl3-pretreated spent coffee grounds using CO2 as a reaction medium. Energy Convers Manag 127:437–442

28. Müsellim E, Tahir MH, Ahmad MS, Ceylan S (2018) Thermokinetic and TG/DSC-FTIR study of pea waste biomass pyrolysis. Appl Therm Eng 137:54–61

29. Nowicki L, Ledakowicz S (2014) Comprehensive characterization of thermal decomposition of sewage sludge by TG–MS. J Anal Appl Pyrolysis 110:220–228

30. Aslan DI, Özoğul B, Ceylan S, Geyikçi F (2018) Thermokinetic analysis and product characterization of medium density fiberboard pyrolysis. Bioresour Technol 258:105–110

31. Ceylan S, Topçu Y (2014) Pyrolysis kinetics of hazelnut husk using thermogravimetric analysis. Bioresour Technol 156:182–188

32. Alwani MS, Khalil HPSA, Sulaiman O et al (2014) An approach to using agricultural waste fibres in biocomposites application: thermogravimetric analysis and activation energy study. BioResources 9:218–230

33. Slopiecka K, Bartocci P, Fantozzi F (2012) Thermogravimetric analysis and kinetic study of poplar wood pyrolysis. Appl Energy 97:491–497

34. E1756–08 A (2015) Standard test method for determination of total solids in biomass. American Society for Testing and Materials West Conshohocken, PA

35. ASTM A (2007) Standard E1755–01. Stand Method Determ Ash Biomass, ASTM Int Philadelphia, USA

36. E872–82 A (2013) Standard test method for volatile matter in the analysis of particulate wood fuels

37. Sadhukhan AK, Gupta P, Saha RK (2009) Modelling of pyrolysis of large wood particles. Bioresour Technol 100:3134–3139

38. Idris SS, Rahman NA, Ismail K (2012) Combustion characteristics of Malaysian oil palm biomass, sub-bituminous coal and their respective blends via thermogravimetric analysis (TGA). Bioresour Technol 123:581–591

39. Cai J, Bi L (2009) Kinetic analysis of wheat straw pyrolysis using isoconversional methods. J Therm Anal Calorim 98:325–330

40. Doyle CD (1965) Series approximations to the equation of thermogravimetric data. Nature 207:290–291

41. Friedman HL (1964) Kinetics of thermal degradation of char-forming plastics from thermogravimetry. Application to a phenolic plastic. In: Journal of polymer science part C: polymer symposia. Wiley Online Library, pp 183–195

42. Kissinger HE (1957) Reaction kinetics in differential thermal analysis. Anal Chem 29:1702–1706

43. Vand V (1943) A theory of the irreversible electrical resistance changes of metallic films evaporated in vacuum. Proc Phys Soc 55:222–246

44. Bhavanam A, Sastry RC (2015) Kinetic study of solid waste pyrolysis using distributed activation energy model. Bioresour Technol 178:126–131

45. Ceylan S, Kazan D (2015) Pyrolysis kinetics and thermal characteristics of microalgae Nannochloropsis oculata and Tetraselmis sp. Bioresour Technol 187:1–5

46. Mishra RK, Mohanty K (2018) Pyrolysis kinetics and thermal behavior of waste sawdust biomass using thermogravimetric analysis. Bioresour Technol 251:63–74

47. Soria-Verdugo A, Garcia-Gutierrez LM, Blanco-Cano L, Garcia-Hernando N, Ruiz-Rivas U (2014) Evaluating the accuracy of the distributed activation energy model for biomass devolatilization curves obtained at high heating rates. Energy Convers Manag 86:1045–1049

48. Ahmad MS, Mehmood MA, Al Ayed OS et al (2017) Kinetic analyses and pyrolytic behavior of Para grass (Urochloa mutica) for its bioenergy potential. Bioresour Technol 224:708–713

49. Fernandes ERK, Marangoni C, Souza O, Sellin N (2013) Thermochemical characterization of banana leaves as a potential energy source. Energy Convers Manag 75:603–608

50. Sait HH, Hussain A, Salema AA, Ani FN (2012) Pyrolysis and combustion kinetics of date palm biomass using thermogravimetric analysis. Bioresour Technol 118:382–389

51. Balogun AO, Lasode OA, McDonald AG (2018) Thermochemical and pyrolytic analyses of Musa spp. residues from the rainforest belt of Nigeria. Environ Prog Sustain Energy 37:1932–1941

52. Singh RK, Pandey D, Patil T, Sawarkar AN (2020) Pyrolysis of banana leaves biomass: physico-chemical characterization, thermal decomposition behavior, kinetic and thermodynamic analyses. Bioresour Technol 123464

53. Yang H, Yan R, Chen H, Lee DH, Zheng C (2007) Characteristics of hemicellulose, cellulose and lignin pyrolysis. Fuel 86:1781–1788

54. Mohamad S, Bakar NKA, Ishak AR et al (2014) Removal of phosphate by paper mill sludge: adsorption isotherm and kinetic study. Asian J Chem 26:3545–3552

55. Yaras A, Arslanoğlu H (2017) Valorization of paper mill sludge as adsorbent in adsorption process of copper (II) ion from synthetic solution: kinetic, isotherm and thermodynamic studies. Arab J Sci Eng:1–10

56. Naqvi SR, Uemura Y, Yusup S, Sugiura Y, Nishiyama N (2015) In situ catalytic fast pyrolysis of paddy husk pyrolysis vapors over MCM-22 and ITQ-2 zeolites. J Anal Appl Pyrolysis 114:32–39

57. White JE, Catallo WJ, Legendre BL (2011) Biomass pyrolysis kinetics: a comparative critical review with relevant agricultural residue case studies. J Anal Appl Pyrolysis 91:1–33

58. Yang H, Yan R, Chen H, Zheng C, Lee DH, Liang DT (2006) In-depth investigation of biomass pyrolysis based on three major components: hemicellulose, cellulose and lignin. Energy Fuel 20:388–393

59. Chen G, He S, Cheng Z, Guan Y, Yan B, Ma W, Leung DYC (2017) Comparison of kinetic analysis methods in thermal decomposition of cattle manure by themogravimetric analysis. Bioresour Technol 243:69–77

60. Yuan X, He T, Cao H, Yuan Q (2017) Cattle manure pyrolysis process: kinetic and thermodynamic analysis with isoconversional methods. Renew Energy 107:489–496

61. Huang X, Cao J-P, Zhao X-Y, Wang JX, Fan X, Zhao YP, Wei XY (2016) Pyrolysis kinetics of soybean straw using thermogravimetric analysis. Fuel 169:93–98

62. Chen J, Liu J, He Y, Huang L, Sun S, Sun J, Chang KL, Kuo J, Huang S, Ning X (2017) Investigation of co-combustion characteristics of sewage sludge and coffee grounds mixtures using thermogravimetric analysis coupled to artificial neural networks modeling. Bioresour Technol 225:234–245

63. Xu Y, Chen B (2013) Investigation of thermodynamic parameters in the pyrolysis conversion of biomass and manure to biochars using thermogravimetric analysis. Bioresour Technol 146:485–493

64. Khan AS, Man Z, Bustam MA, Kait CF, Ullah Z, Nasrullah A, Khan MI, Gonfa G, Ahmad P, Muhammad N (2016) Kinetics and thermodynamic parameters of ionic liquid pretreated rubber wood biomass. J Mol Liq 223:754–762

65. Kim YS, Kim YS, Kim SH (2010) Investigation of thermodynamic parameters in the thermal decomposition of plastic waste− waste lube oil compounds. Environ Sci Technol 44:5313–5317